

# Topological superconductivity in quantum wires mediated by helical magnons

Florinda Viñas Boström<sup>1,2,\*</sup> and Emil Viñas Boström<sup>3,4,†</sup>

<sup>1</sup>*Institut für Mathematische Physik, Technische Universität Braunschweig, D-38106 Braunschweig, Germany*

<sup>2</sup>*Division of Solid State Physics and NanoLund, Lund University, Box 118, S-221 00 Lund, Sweden*

<sup>3</sup>*Nano-Bio Spectroscopy Group, Departamento de Física de Materiales, Universidad del País Vasco, 20018 San Sebastian, Spain*

<sup>4</sup>*Max Planck Institute for the Structure and Dynamics of Matter, Luruper Chaussee 149, 22761 Hamburg, Germany*

(Dated: December 6, 2023)

Triplet superconductivity arises in systems where the effective electronic attraction favors Cooper pairs with a symmetric spin structure, as may occur in non-collinear magnetic systems. Here we show that topological triplet superconductivity can be realized in a one-dimensional quantum wire through the interaction with magnetic fluctuations of a helical magnet. The magnon-mediated attraction favors triplet superconductivity over a large sector of magnetic parameters, and stabilizes a topological phase with a superconducting gap of the order of 1 meV over an extended region of chemical potentials.

A promising path to realize fault-tolerant quantum computing is to utilize the excitations of topologically ordered systems [1–3]. These excitations, generically named anyons [4, 5], are predicted to appear across a wide range of platforms, such as fractional quantum Hall systems, quantum spin liquids, and topological superconductors [6–10]. In particular, the sub-class of excitations called non-abelian anyons allow for information to be non-locally encoded and processed in the braiding patterns of the anyon world lines [2, 3]. In topological superconductors, non-abelian anyons appear at the edges or in vortex cores of chiral two-dimensional superconductors [11–17], and at the ends of one-dimensional (1-D) quantum wires [18–21]. However, due to the difficulties associated with realizing such phases, conclusive evidence of topological superconductivity has not been found in any experimental platform.

It has recently been proposed that chiral topological superconductivity can be realized in two-dimensional heterostructures [22–28], where itinerant electrons interact with a non-collinear magnetic structure, or in chains of magnetic atoms deposited on a conventional superconductor [29–32]. In 1-D systems, superconductors with triplet ( $p$ -wave) pairing are known to always reside in a topological class that can host non-trivial topological phases [33–35]. To engineer topological superconductivity in 1-D, the dominant approach has been to combine proximity-induced  $s$ -wave superconductivity with strong spin-orbit coupling (SOC) semi-conductors and time-reversal symmetry breaking magnetic fields [11, 36–47]. Although straightforward in principle, this approach is in practice associated with a number of challenges, the most prominent being that the time-reversal breaking field must be finely tuned such that it is large enough to realize an effective spin-polarized regime, but small enough not to suppress the effective superconducting gap [11, 19, 20]. To avoid this problem it would be desir-

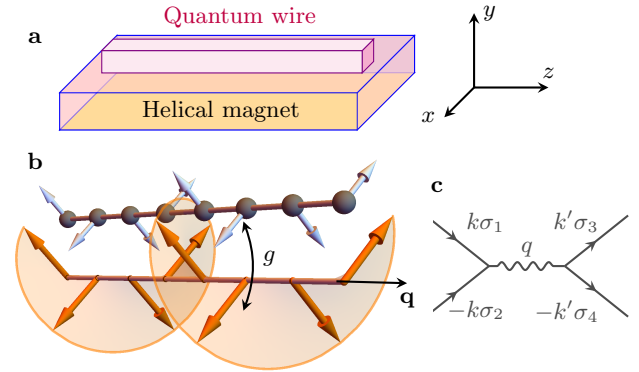


FIG. 1. Principles of magnon-mediated superconductivity. **a**, Experimental setup with a quantum wire in proximity to a helical magnet. **b**, The helical magnetic order (orange arrows) induces an effective spin-orbit interaction and Zeeman splitting of the electronic bands via the spin-electron coupling  $g$ . Magnon fluctuations around the equilibrium magnetic order provide an effective attractive interaction among the electrons (blue arrows). **c**, Due to the non-collinear magnetic structure, magnon fluctuations mediate scattering between electrons with arbitrary spin projections  $\sigma_i$ .

able to find a protocol for topological superconductivity where the spin-polarized regime and the superconducting gap both are increasing functions of some control parameter.

To address this challenge, we here propose a platform to stabilize triplet superconductivity by coupling a quantum wire to a helical magnet (see Fig. 1). The non-collinear magnetic order induces an effective SOC and Zeeman field among the electrons (see Fig. 2), thereby realizing an effective single-band regime. The magnon excitations of the helical magnet further mediate an effective attractive interaction between the electrons, which stabilizes triplet superconductivity with a superconduct-

ing gap of the order of 1 meV over a large portion of the magnetic phase space. Within the effective single-band regime, the system enters a topological phase, with unpaired Majorana bound states at each end of the wire. Crucially, both the size of the effective single-band regime and the superconducting gap are increasing functions of the spin-electron coupling  $g$ . Our proposal thereby identifies quantum wires in proximity to helical magnets as a promising platform to explore topological superconductivity in 1-D.

To investigate magnon-mediated superconductivity in a quantum wire, we consider an interacting system of spins and electrons described by the lattice Hamiltonian

$$H = -t \sum_{\langle ij \rangle \sigma} \hat{c}_{i\sigma}^\dagger \hat{c}_{j\sigma} - J \sum_{\langle ij \rangle} \hat{\mathbf{S}}_i \cdot \hat{\mathbf{S}}_j - \sum_{\langle ij \rangle} \mathbf{D}_{ij} \cdot (\hat{\mathbf{S}}_i \times \hat{\mathbf{S}}_j) - g \sum_i \hat{\mathbf{s}}_i \cdot \hat{\mathbf{S}}_i. \quad (1)$$

Here  $\hat{c}_{i\sigma}$  destroys an electron at site  $i$  and of spin projection  $\sigma$ , and  $\hat{\mathbf{S}}_i$  is the spin operator at site  $i$  for a spin of magnitude  $S$ . The parameters  $t$ ,  $J$ , and  $\mathbf{D}$  respectively determine the nearest-neighbor electronic hopping amplitude, the exchange interaction, and the antisymmetric Dzyaloshinskii-Moriya interaction (DMI). The spins and electrons interact via a local spin-electron coupling of strength  $g$ , and the electronic spin operator is defined by  $\hat{\mathbf{s}}_i = \sum_{\sigma\sigma'} \hat{c}_{i\sigma}^\dagger \boldsymbol{\tau}_{\sigma\sigma'} \hat{c}_{i\sigma'}$ , with  $\boldsymbol{\tau}$  the Pauli matrix vector.

The competition between exchange and DMI stabilizes a helical magnetic order, characterized by a propagation vector  $\mathbf{q}$  and a vector  $\hat{\mathbf{n}}$  defining the plane of polarization. Specifically, the magnitude of the spiral momentum is given by  $\sqrt{2} \tan q = D/J$ , while the directions of the momentum and polarization vectors are determined by the normalized DMI vector  $\hat{\mathbf{D}}$ . Here we consider a DMI such that the spiral momentum  $\mathbf{q}$  lies along the wire axis  $\hat{\mathbf{z}}$ , and with  $\hat{\mathbf{n}}$  parallel to  $\mathbf{q}$  (see Fig. 1). The equilibrium spin texture is then a spin helix, and can be written as  $\mathbf{S}_i = \cos(\mathbf{q} \cdot \mathbf{r}_i) \mathbf{e}_1 + \sin(\mathbf{q} \cdot \mathbf{r}_i) \mathbf{e}_2$ , where the vectors  $\mathbf{e}_\alpha$  and  $\hat{\mathbf{n}}$  define a right-handed orthonormal system [48].

In the following the magnetic texture is assumed to be commensurate with the electronic lattice, such that the spin spiral is periodic over a distance  $La$ , where  $L$  is an integer and  $a$  is the electronic lattice parameter. To describe fluctuations around the equilibrium order, the spin operators  $\hat{\mathbf{S}}_i$  are expressed in terms of a set of bosonic operators by performing a Holstein-Primakoff expansion around the local spin axis  $\mathbf{S}_i$  [48]. This results in a diagonal magnon Hamiltonian  $H_m = \sum_{np} \Omega_{np} \alpha_{np}^\dagger \alpha_{np}$ , where  $\Omega_{np}$  is the energy of a magnon with momentum  $p$  in band  $n$ . The momentum runs over the magnetic Brillouin zone  $[-\pi/La, \pi/La]$ , and the number of magnon bands is  $L$ .

There are two main effects of the spin spiral on the electronic structure: First, the coupling to the equilibrium magnetic structure  $\mathbf{S}_i$  induces an effective SOC and Zeeman splitting of the electronic bands (see Fig. 2a).

Second, the coupling to magnon fluctuations around the helical configuration generates an effective attractive interaction among the electrons, which ultimately leads to superconductivity. The effect of the static spin spiral can be exactly accounted for, by diagonalizing the electronic sub-system in presence of the spiral  $\mathbf{S}_i$  [48, 49], and results in the electron Hamiltonian  $H_e = \sum_{k\tau} \epsilon_{k\tau} d_{k\tau}^\dagger d_{k\tau}$ . Here  $\tau$  denotes the electronic bands, and the momentum runs over the electronic Brillouin zone  $[-\pi/a, \pi/a]$ . The spiral shifts the minima of the originally spin-degenerate bands to  $\pm q/2$  (Fig. 2a), thereby inducing an effective Rashba SOC. This shift is independent of the value of  $g$ , and is set for any finite  $g$  by the momentum of the spin spiral. In addition, the coupling opens a gap of size  $\Delta_b = 2gS$  at  $k = 0$  and  $k = \pm\pi/a$ , acting like an effective Zeeman field. Together these effects realize an effective single-band regime for chemical potentials inside the gap.

The electron-magnon interaction is found by expressing the spin-electron coupling (the last term in Eq. 1) in terms of the magnon and band electron operators. Due to the non-collinear structure of the spin spiral, the coupling has a non-trivial spin structure (see Fig. 1c), and in general gives rise to magnon-mediated scattering between electrons with arbitrary spin projections. An effective electron-electron interaction is obtained by integrating out the magnons within a finite temperature functional integral formulation [48]. The effective interaction  $U_{\tau_1\tau_2}^{\tau_3\tau_4}(k, k')$  implicitly depends on the magnetic structure via the spin-electron coupling  $g$ , the spiral momentum  $q$ , and the transformation matrices used to diagonalize the magnon and electron sub-systems. In the static limit the superconducting gap  $\Delta_k^{\tau\tau'}$  is determined via the linearized gap equation

$$\Delta_k^{\tau_1\tau_2} = \sum_{k'\tau_3\tau_4} U_{\tau_1\tau_2}^{\tau_3\tau_4}(k, k') \left( \sum_{\tau} \frac{\tanh(\beta \xi_{k'\tau})}{2\xi_{k'\tau}} \right) \Delta_{k'}^{\tau_3\tau_4}, \quad (2)$$

where  $\beta = 1/(k_B T)$  is the inverse temperature, and  $\xi_k = \epsilon_k - \mu$ . The gap equation can be viewed as an eigenvalue problem for the susceptibility matrix  $\chi_{\tau_1\tau_2}^{\tau_3\tau_4}(k, k')$ , implicitly defined by the right hand side of Eq. 2, and superconductivity is signaled by the largest eigenvalue of this matrix exceeding unity.

On the mean-field level the electronic Hamiltonian is of the Bogoliubov-de Gennes (BdG) form, and can be written as  $H = \sum_k \Phi_k^\dagger \mathcal{H}_k \Phi_k$  with  $\mathcal{H}_k$  as a  $4 \times 4$  matrix [48]. The gap  $\Delta_{\tau\tau'}$  can be decomposed into four components, given by the singlet gap  $\Delta_s = (\Delta_{du} - \Delta_{ud})/2$  and the triplet gaps  $\Delta_u = \Delta_{uu}$ ,  $\Delta_d = \Delta_{dd}$ , and  $\Delta_p = (\Delta_{du} + \Delta_{ud})/2$ . The subscripts  $u$  and  $d$  refer to the band index  $\tau$ , which can be viewed as an effective spin index, where  $u$  ( $d$ ) denotes the upper (lower) band or effective spin up (down). Due to the fermionic nature of the electronic operators, the singlet and triplet gaps are even and odd functions of  $k$ , respectively.

We begin with analyzing how the symmetry of the

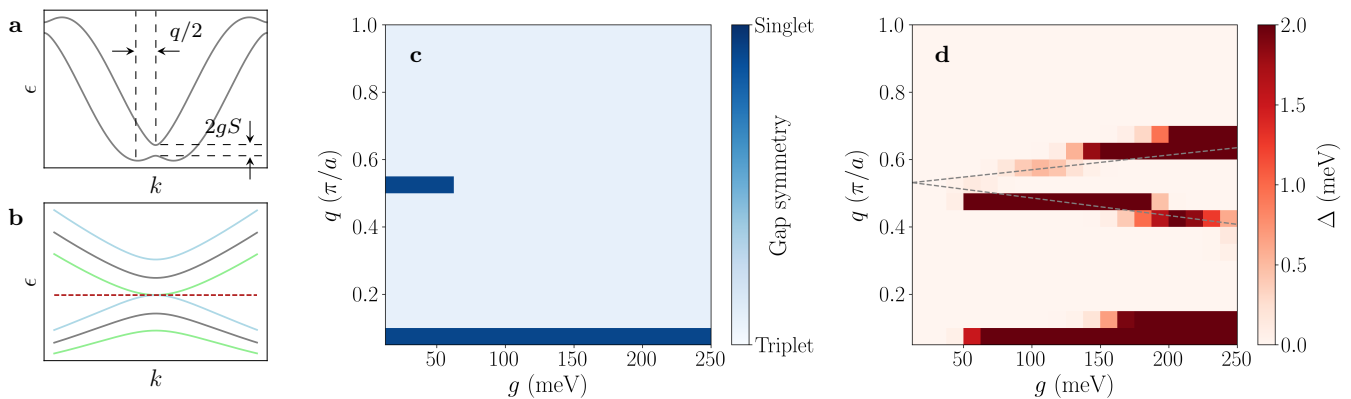


FIG. 2. Parameter dependence of magnon-mediated superconductivity. **a**, Electronic band structure for a spin-electron coupling  $g = 150$  meV and a spiral momentum  $q = \pi/3a$ . **b**, Electronic band structure around  $k = 0$  for a spin-electron coupling  $g = 150$  meV and spiral momenta  $q = 0.44\pi/a$  (green),  $q = 0.5\pi/a$  (gray) and  $q = 0.57\pi/a$  (blue). The red dashed line indicates the chemical potential  $\mu = -1.4$  eV. **c**, Symmetry of the dominant superconducting gap as a function of spin-electron coupling  $g$  and spiral momentum  $q$ , for a chemical potential  $\mu = -1.4$  eV. **d**, Magnitude of the dominant superconducting gap as a function of spin-electron coupling  $g$  and spiral momentum  $q$ , for a chemical potential  $\mu = -1.4$  eV. The gray dashed lines indicate the positions of the van Hove singularities. In all panels the spin length is  $S = 1$ , the electronic hopping is  $t = 1$  eV, and the exchange interaction is  $J = 10$  meV.

dominant superconducting gap depends on the spiral momentum  $q$ , the spin-electron coupling  $g$ , and the chemical potential  $\mu$ . For parameters such that the energy difference  $\epsilon_u(k_{Fu}) - \epsilon_d(k_{Fd}) \gg \Omega$ , with  $k_{F\tau}$  the Fermi momentum in band  $\tau$ , and  $\Omega$  a typical magnon energy, Cooper pairs will predominantly form from states within the same band. In this regime, the gap function becomes diagonal in the band indexes. At temperatures below 10 K, the pairing interaction is highly restricted to the Fermi surface, which for a 1-D system consists of the points  $\pm k_{F\tau}$ . Restricting the gap equation to the Fermi surface, and neglecting contributions from inter-band scattering, Eq. 2 reduces to a  $2 \times 2$  matrix problem and can be solved analytically [48]. The eigenvalues of the susceptibility matrix are  $\lambda_s = \chi(k_F, k_F) + \chi(k_F, -k_F)$  and  $\lambda_p = \chi(k_F, k_F) - \chi(k_F, -k_F)$ , for singlet and triplet pairing, respectively. These solutions show that the sign of the term  $\chi(k_F, -k_F)$ , accounting for scattering between the points  $k_F$  and  $-k_F$ , determines the symmetry of the dominant gap. Since only triplet pairing is consistent with the symmetry of intra-band Cooper pairs, a consistent superconducting solution requires  $\lambda_p > \lambda_s$ . When  $\epsilon_u(k_{Fu}) - \epsilon_d(k_{Fd}) \lesssim \Omega$ , inter-band scattering becomes important, and the dominant superconducting gap is expected to have  $s$ -wave symmetry.

This qualitative analysis is in good agreement with the numerical solution of Eq. 2, showing that the dominant superconducting gap has triplet symmetry over a large fraction of the phase diagram (see Fig. 2b). Only in regions where  $\epsilon_u(k_{Fu}) - \epsilon_d(k_{Fd}) \lesssim \Omega$ , such as close to the ferromagnetic limit  $q = 0$ , or when both  $k_{F\tau}$  are close to the band edges (around  $k_{F\tau} = 0$ ), does the dominant gap have singlet symmetry. In the strict ferromagnetic limit,

this result can be established analytically [48], by noting that ferromagnetic magnons only scatter electrons with opposite spins. That such a large portion of the phase diagram is dominated by triplet pairing follows from the fact that singlet pairing requires inter-band scattering. For  $k_{Fd} \neq k_{Fu}$ , such scattering results in Cooper pairs with a finite center-of-mass momentum  $k_{Fu} - k_{Fd} \sim q$ , which strongly suppresses singlet pairing at finite  $q$  [50]. With increasing  $q$ , intra-band magnon scattering therefore quickly becomes the dominant pairing mechanism, resulting in a gap with triplet symmetry. We note that in the antiferromagnetic limit  $q = \pi$ , an effective gap opens between the electronic bands, and only triplet pairing is possible.

We now analyze how the magnitude of the dominant superconducting gap depends on the magnetic parameters. In the regime  $\epsilon_u(k_{Fu}) - \epsilon_d(k_{Fd}) \gg \Omega$ , where inter-band scattering can be neglected, the zero temperature mean-field gap is given by  $\Delta = 2\Omega e^{-1/(\rho_F U)}$  [48]. Here  $\rho_F$  is the electronic density of states (DOS) at the Fermi level, and  $U = U(k, k) - U(k, -k)$  the effective pairing interaction in the triplet sector. Since  $U \sim g^2/\Omega$ , the superconducting gap is expected to increase exponentially with the spin-electron coupling. To estimate  $\Delta$ , we note that for an approximately linear dispersion, the electronic DOS tends to the constant  $\rho_0 = 1/(4\pi t)$ , while close to a band edge at energy  $\epsilon_0$  van Hove singularities of the form  $\rho(\epsilon) = \rho_0 \sqrt{t/(\epsilon - \epsilon_0)}$  develop. Approximating  $U$  with its value in the ferromagnetic limit,  $U = 4g^2 S/\Omega$ , the dimensionless coupling strength is  $\lambda_{\text{eff}} = \rho_F U \approx g^2 S/(\pi t \Omega)$ . For the typical values  $S = 1$ ,  $t = 1$  eV and  $\Omega = 10$  meV, a spin-electron coupling of  $g = 100$  meV gives a gap of  $\Delta \sim 1$  meV, with significant enhancements expected at

the van Hove singularities.

The magnitude of the superconducting gap is also obtained from a numerical solution of Eq. 2, whose largest eigenvalue  $\lambda$  is related to the gap by  $\Delta = 2\Omega e^{-1/\lambda}$ . The magnitude of  $\Delta$  is shown in Fig. 2d, and is found to generally increase with  $g$  as anticipated above. However, it also displays a clear non-monotonic behavior with  $g$ , which can be attributed to the variation of the electronic DOS with the magnetic parameters. In particular, a gap between the upper and lower bands opens at  $k = 0$  as a function of  $g$ , whose position varies with the spiral momentum  $q$  (see Fig. 2b). For constant chemical potential, as assumed in Figs. 2c and 2d, the DOS at the Fermi level therefore changes both with  $g$  and  $q$ , and is significantly enhanced at the van Hove singularities forming at the band edges. The diagonal lines in Fig. 2d, emanating from  $q \approx \pi/(2a)$ , trace the van Hove singularities as a function of  $g$ . The overall magnitude of the gap, of order  $\Delta \sim 1$  meV, is in line with the estimate above.

We now investigate the topological phases of the superconducting wire. In the effective single-band limit, where the chemical potential lies inside the band gap, the BdG Hamiltonian maps directly onto the Hamiltonian of the Kitaev chain [34]. This system is known to permit a topologically non-trivial phase with unpaired Majorana bound states appearing at each end of the quantum wire. Since the effective single-band limit of the model discussed here can be connected to the Kitaev model by continuously deforming the dispersion and gap function, its topological phase diagram is identical to the Kitaev model [20, 48]. It can be constructed by counting the number of intersections  $N$  between a line at constant chemical potential and the dispersion, with the topological index given by  $\mathbb{Z}_2 = (N/2) \bmod 2$ .

To obtain the topological phase diagram of the full two-band model, we first consider the case where  $\Delta_u \neq 0$  and  $\Delta_d \neq 0$  but  $\Delta_s = \Delta_p = 0$ . In this limit, the model corresponds to two independent copies of the Kitaev model, and a  $\mathbb{Z}_2$  invariant can be defined separately for each band. Denoting these invariants by  $\mathbb{Z}_d$  and  $\mathbb{Z}_u$ , the  $\mathbb{Z}_2$  index of the full system is given by  $\mathbb{Z}_d \mathbb{Z}_u$ . Since adding finite inter-band pairings cannot close the superconducting gap, the full two-band model is continuously connected to the  $\Delta_s = \Delta_p = 0$  limit, and for  $\Delta_u \neq 0$  and  $\Delta_d \neq 0$  the phase diagram can be constructed by counting the number of times  $N$  a line at constant chemical potential crosses the bands  $\epsilon_{k\tau}$  (with  $\mathbb{Z}_2 = (N/2) \bmod 2$ , see Fig. 3). For  $g = 0$  the system is always in a trivial regime, while for  $g \neq 0$  two regions with non-trivial topology grow out of the upper and lower band edges. The size of these regions increase linearly with the magnitude of  $g$ . We note that in the antiferromagnetic limit the system is always in the trivial phase, since there is no effective single-band regime in this case.

Our results demonstrate that topological superconductivity is stabilized whenever the quantum wire is in an

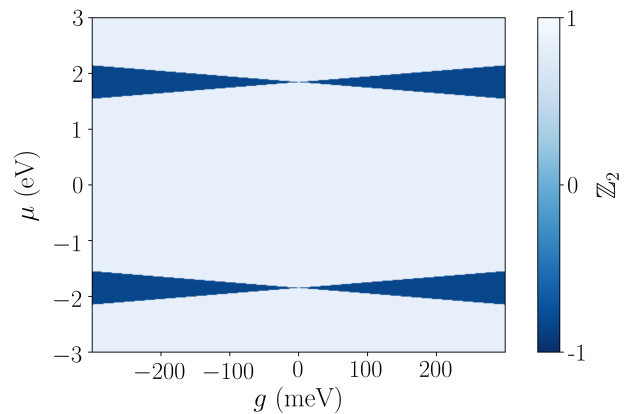


FIG. 3. Topological phase diagram of magnon-mediated superconductivity as a function of spin-electron coupling  $g$  and chemical potential  $\mu$ . The magnetic spiral has a wave length  $L = 8$  and momentum  $q = \pi/(4a)$ . The light regions show the trivial phase, while the dark regions correspond to a topological phase. The spin length is  $S = 1$  and the electronic hopping  $t = 1$  eV.

effective single-band regime. Such a regime can be experimentally realized by placing the chemical potential inside the  $k = 0$  or  $k = \pm\pi/a$  band gap  $\Delta_b$ , induced by the coupling to the spiral. Magnon scattering further opens a superconducting gap  $\Delta$ , whose magnitude is shown in Fig. 2c and is approximately determined by the product  $g^2 \rho_F / \Omega$ . To favor topological superconductivity, it is desirable to find a system with a large  $g$  and  $\rho_F$ , but a small  $\Omega$  (however not too small, since  $\Omega$  sets the upper limit of  $\Delta$ ).

To realize the model of Eq. 1, several strategies are possible. The most straightforward is to consider a quantum wire in proximity to a helical magnet, as illustrated in Fig. 1. In this case, the wire could consist either of a simple metal, or a lightly doped or gate tuned semiconductor (such as InAs [51, 52]), with a single active and largely uncorrelated band. For the helical magnet, it is preferable to use a material with a short spiral wave length ( $\lambda \sim 10$  nm), low magnon energy and large spin length, such as MnGe, MnSi or NiI<sub>2</sub> [53, 54]. To maximize  $g$ , it is desirable to use a wire geometry where as much as possible of the wire is strongly coupled to the magnet. Estimating  $g$  for a general interface is hard, but based on earlier work it is expected that  $g \sim 10$ – $100$  meV can be achieved [55–58].

We have demonstrated that magnon fluctuations of a helical magnet can mediate triplet superconductivity in a proximate quantum wire. As the induced band gap and superconducting gap both increase with the spin-electron coupling  $g$ , various material engineering techniques such as wire geometry optimization, microstructuring or cavity-enhanced light-matter couplings can be employed to maximize its value [51, 59–62]. We expect that, utilizing such strategies, an effective cou-

pling exceeding  $g \approx 50$  meV can be achieved, allowing our protocol to surpass present state-of-the-art experiments with a topological superconducting gap of the order  $\Delta \sim 0.1$  meV [47]. The present model is a simplified description of a real quantum wire, and in reality effects coming from repulsive electron-electron interactions, disorder and a more complex band structure should be included [63]. While the former is expected to compete with the magnon-mediated attraction, the later could result in a larger DOS at the Fermi level, thereby enhancing superconductivity. In conclusion, our results identify quantum wires in proximity to non-collinear magnets as a promising platform to explore topological superconductivity in 1-D.

We acknowledge fruitful discussions with Oladunjoye A. Awoga. FVB acknowledges funding from the Swedish Research Council (VR), and EVB acknowledges funding from the European Union's Horizon Europe research and innovation programme under the Marie Skłodowska-Curie grant agreement No 101106809.

---

\* florinda.vinas.bostrom@ftf.lth.se

† emil.bostrom@mpsd.mpg.de

- [1] X. G. Wen and Q. Niu, *Phys. Rev. B* **41**, 9377 (1990).
- [2] A. Kitaev, *Annals of Physics* **303**, 2 (2003).
- [3] C. Nayak, S. H. Simon, A. Stern, M. Freedman, and S. Das Sarma, *Rev. Mod. Phys.* **80**, 1083 (2008).
- [4] J. M. Leinaas and J. Myrheim, *Il Nuovo Cimento B Series* **11** **37**, 1–23 (1977).
- [5] F. Wilczek, *Phys. Rev. Lett.* **49**, 957 (1982).
- [6] D. Arovas, J. R. Schrieffer, and F. Wilczek, *Phys. Rev. Lett.* **53**, 722 (1984).
- [7] A. Kitaev, *Annals of Physics* **321**, 2 (2006).
- [8] L. Savary and L. Balents, *Reports on Progress in Physics* **80**, 016502 (2016).
- [9] H. Bartolomei, M. Kumar, R. Bisognin, A. Marguerite, J.-M. Berroir, E. Bocquillon, B. Plaçaïs, A. Cavanna, Q. Dong, U. Gennser, Y. Jin, and G. Fève, *Science* **368**, 173 (2020).
- [10] J. Nakamura, S. Liang, G. C. Gardner, and M. J. Manfra, *Nature Physics* **16**, 931 (2020).
- [11] L. Fu and C. L. Kane, *Phys. Rev. Lett.* **100**, 096407 (2008).
- [12] S. Nakosai, Y. Tanaka, and N. Nagaosa, *Phys. Rev. B* **88**, 180503 (2013).
- [13] H.-H. Sun, K.-W. Zhang, L.-H. Hu, C. Li, G.-Y. Wang, H.-Y. Ma, Z.-A. Xu, C.-L. Gao, D.-D. Guan, Y.-Y. Li, C. Liu, D. Qian, Y. Zhou, L. Fu, S.-C. Li, F.-C. Zhang, and J.-F. Jia, *Phys. Rev. Lett.* **116**, 257003 (2016).
- [14] G. C. Ménard, S. Guissart, C. Brun, R. T. Leriche, M. Trif, F. Debontridder, D. Demaille, D. Roditchev, P. Simon, and T. Cren, *Nature Communications* **8** (2017), 10.1038/s41467-017-02192-x.
- [15] A. Palacio-Morales, E. Mascot, S. Cocklin, H. Kim, S. Rachel, D. K. Morr, and R. Wiesendanger, *Science Advances* **5** (2019), 10.1126/sciadv.aav6600.
- [16] Z. Wang, J. O. Rodriguez, L. Jiao, S. Howard, M. Graham, G. D. Gu, T. L. Hughes, D. K. Morr, and V. Mahavan, *Science* **367**, 104–108 (2020).
- [17] S. Kezilebieke, M. N. Huda, V. Vaño, M. Aapro, S. C. Ganguli, O. J. Silveira, S. Głodzik, A. S. Foster, T. Ojanen, and P. Liljeroth, *Nature* **588**, 424–428 (2020).
- [18] K. Flensberg, *Phys. Rev. B* **82**, 180516 (2010).
- [19] Y. Oreg, G. Refael, and F. von Oppen, *Phys. Rev. Lett.* **105**, 177002 (2010).
- [20] R. M. Lutchyn, J. D. Sau, and S. Das Sarma, *Phys. Rev. Lett.* **105**, 077001 (2010).
- [21] R. M. Lutchyn, E. P. A. M. Bakkers, L. P. Kouwenhoven, P. Krogstrup, C. M. Marcus, and Y. Oreg, *Nature Reviews Materials* **3**, 52–68 (2018).
- [22] G. Yang, P. Stano, J. Klinovaja, and D. Loss, *Phys. Rev. B* **93**, 224505 (2016).
- [23] S. Rex, I. V. Gornyi, and A. D. Mirlin, *Phys. Rev. B* **100**, 064504 (2019).
- [24] J. Bedow, E. Mascot, T. Posske, G. S. Uhrig, R. Wiesendanger, S. Rachel, and D. K. Morr, *Phys. Rev. B* **102**, 180504 (2020).
- [25] S. A. Díaz, J. Klinovaja, D. Loss, and S. Hoffman, *Phys. Rev. B* **104**, 214501 (2021).
- [26] K. Mæland and A. Sudbø, *Phys. Rev. Res.* **4**, L032025 (2022).
- [27] K. Mæland and A. Sudbø, *Phys. Rev. Lett.* **130**, 156002 (2023).
- [28] K. Mæland, S. Abnar, J. Benestad, and A. Sudbø, “Topological superconductivity mediated by magnons of helical magnetic states,” (2023), arXiv:2309.07211.
- [29] S. Nadj-Perge, I. K. Drozdov, J. Li, H. Chen, S. Jeon, J. Seo, A. H. MacDonald, B. A. Bernevig, and A. Yazdani, *Science* **346**, 602–607 (2014).
- [30] J. Neuhaus-Steinmetz, E. Y. Vedmedenko, T. Posske, and R. Wiesendanger, *Phys. Rev. B* **105**, 165415 (2022).
- [31] L. Schneider, P. Beck, L. Rózsa, T. Posske, J. Wiebe, and R. Wiesendanger, *Nature Communications* **14**, 2742 (2023).
- [32] O. A. Awoga, I. Ioannidis, A. Mishra, M. Leijnse, M. Trif, and T. Posske, “Controlling majorana hybridization in magnetic chain-superconductor systems,” (2023), arXiv:2308.07961 [cond-mat.mes-hall].
- [33] A. Altland and M. R. Zirnbauer, *Phys. Rev. B* **55**, 1142 (1997).
- [34] A. Y. Kitaev, *Physics-Uspekhi* **44**, 131 (2001).
- [35] C.-K. Chiu, J. C. Y. Teo, A. P. Schnyder, and S. Ryu, *Rev. Mod. Phys.* **88**, 035005 (2016).
- [36] K. T. Law, P. A. Lee, and T. K. Ng, *Phys. Rev. Lett.* **103**, 237001 (2009).
- [37] T. D. Stanescu, R. M. Lutchyn, and S. Das Sarma, *Phys. Rev. B* **84**, 144522 (2011).
- [38] J. Alicea, Y. Oreg, G. Refael, F. von Oppen, and M. P. A. Fisher, *Nature Physics* **7**, 412 (2011).
- [39] V. Mourik, K. Zuo, S. M. Frolov, S. R. Plissard, E. P. A. M. Bakkers, and L. P. Kouwenhoven, *Science* **336**, 1003–1007 (2012).
- [40] A. Das, Y. Ronen, Y. Most, Y. Oreg, M. Heiblum, and H. Shtrikman, *Nature Physics* **8**, 887–895 (2012).
- [41] A. D. K. Finck, D. J. Van Harlingen, P. K. Mohseni, K. Jung, and X. Li, *Phys. Rev. Lett.* **110**, 126406 (2013).
- [42] S. M. Albrecht, A. P. Higginbotham, M. Madsen, F. Kuemmeth, T. S. Jespersen, J. Nygård, P. Krogstrup, and C. M. Marcus, *Nature* **531**, 206–209 (2016).
- [43] M. T. Deng, S. Vaitiekėnas, E. B. Hansen, J. Danon, M. Leijnse, K. Flensberg, J. Nygård, P. Krogstrup, and C. M. Marcus, *Science* **354**, 1557–1562 (2016).

- [44] F. Nichele, A. C. C. Drachmann, A. M. Whiticar, E. C. T. O’Farrell, H. J. Suominen, A. Fornieri, T. Wang, G. C. Gardner, C. Thomas, A. T. Hatke, P. Krogstrup, M. J. Manfra, K. Flensberg, and C. M. Marcus, *Phys. Rev. Lett.* **119**, 136803 (2017).
- [45] H. Zhang, D. E. Liu, M. Wimmer, and L. P. Kouwenhoven, *Nature Communications* **10** (2019), 10.1038/s41467-019-13133-1.
- [46] E. Prada, P. San-Jose, M. W. A. de Moor, A. Geresdi, E. J. H. Lee, J. Klinovaja, D. Loss, J. Nygård, R. Aguado, and L. P. Kouwenhoven, *Nature Reviews Physics* **2**, 575–594 (2020).
- [47] M. Aghaee et al. (Microsoft Quantum), *Phys. Rev. B* **107**, 245423 (2023).
- [48] “See supplemental material at [url will be inserted by publisher] for additional details on the diagonalization of the magnon and electron sub-systems, the derivation of the electron-magnon interaction, the derivation of the effective electron-electron interaction, the derivation of the gap equation, and an extended discussion of the  $Z_2$  topological invariant of the superconducting system.”
- [49] E. Viñas Boström, F. G. Eich, and A. Rubio, “Magnon frequency renormalization by the electronic geometrical spin torque in itinerant magnets,” (2021), [arXiv:2112.06547](https://arxiv.org/abs/2112.06547).
- [50] F. Loder, A. P. Kampf, and T. Kopp, *Phys. Rev. B* **81**, 020511 (2010).
- [51] M. Nilsson, F. Viñas Boström, S. Lehmann, K. A. Dick, M. Leijnse, and C. Thelander, *Phys. Rev. Lett.* **121**, 156802 (2018).
- [52] R. Debbarma, M. Aspegren, F. Viñas Boström, S. Lehmann, K. Dick, and C. Thelander, *Phys. Rev. B* **106**, L180507 (2022).
- [53] N. Nagaosa and Y. Tokura, *Nature Nanotechnology* **8**, 899 (2013).
- [54] Q. Song, C. A. Occhialini, E. Ergeçen, B. Ilyas, D. Amoroso, P. Barone, J. Kapeghian, K. Watanabe, T. Taniguchi, A. S. Botana, S. Picozzi, N. Gedik, and R. Comin, *Nature* **602**, 601 (2022).
- [55] Z. Qiao, W. Ren, H. Chen, L. Bellaiche, Z. Zhang, A. H. MacDonald, and Q. Niu, *Phys. Rev. Lett.* **112**, 116404 (2014).
- [56] T. Norden, C. Zhao, P. Zhang, R. Sabirianov, A. Petrou, and H. Zeng, *Nature Communications* **10** (2019), 10.1038/s41467-019-11966-4.
- [57] K. Mæland, H. I. Røst, J. W. Wells, and A. Sudbø, *Phys. Rev. B* **104**, 125125 (2021).
- [58] C. Cardoso, A. T. Costa, A. H. MacDonald, and J. Fernández-Rossier, *Phys. Rev. B* **108**, 184423 (2023).
- [59] P. J. Moll, *Annual Review of Condensed Matter Physics* **9**, 147–162 (2018).
- [60] M. A. Sentef, M. Ruggenthaler, and A. Rubio, *Science Advances* **4** (2018), 10.1126/sciadv.aau6969.
- [61] E. Barrigón, M. Heurlin, Z. Bi, B. Monemar, and L. Samuelson, *Chemical Reviews* **119**, 9170–9220 (2019).
- [62] E. Viñas Boström, A. Sriram, M. Claassen, and A. Rubio, *npj Computational Materials* **9** (2023), 10.1038/s41524-023-01158-6.
- [63] S. Das Sarma, *Nature Physics* (2023), 10.1038/s41567-022-01900-9.